Stabilization of the γ-Sn phase in tin nanoparticles and nanowires

N. G. Hörmann,[1, 2] J. Rohrer,[3] A. Groß,[1, 2] and P. Kaghazchi[4, *]

[1]*Helmholtz Institute Ulm (HIU) Electrochemical Energy Storage, Helmholtzstr. 11, 89069 Ulm*
[2]*Universität Ulm, Institut für Theoretische Chemie, Albert-Einstein-Allee 11, 89069 Ulm*
[3]*Institut fr Materialwissenschaft, Fachgebiet Materialmodellierung,*
Technische Universität Darmstadt, Jovanka-Bontschits-Str. 2, 64287 Darmstadt
[4]*Institut für Chemie und Biochemie, Freie Universität Berlin, Takustr. 3, 14195 Berlin, Germany*
(Dated: February 19, 2015)

The structure of Sn nanoparticles and nanowires are studeied using density functional theory (DFT) in conjuction with theromodynamic considerations as well as *ab initio* molecular dynamics (AIMD). Besides the low-temperature α and room-temperature β phases, the high-temperature γ phase is considered. The calculated temperature-size phase diagram shows that at finite temperatures for sizes smaller than 50 nm, metallic β- and γ-Sn nanoparticles are more stable than semimetallic α-Sn ones. In particular, at room temperature, whereas β-Sn is stable for nanoparticles larger than 10 nm, γ-Sn becomes more stable for nanoparticles of smaller sizes, which is due to the smaller surface energy of the latter phase. Moreover, we find that at room temperature β-Sn nanowires are unstable against a transformation to γ-like nanowires. The $\beta \rightarrow \gamma$ phase transition in nanowires occurs without any kinetic barrier. Our findings suggest that the structure, and thereby, performance of Sn nanostructures in Li-based battery and optoelectronic applications can change under ambient conditions.

I. INTRODUCTION

Tin (Sn) nanoparticles have gained increasing attention in Li-based battery[1–9]. and optoelectronic applications[12–14]. As an anode material, Sn has a much higher capacity than currently-used graphite intercalation anodes. The amount of Li stored per C-atom (1:6), which determines the capacity is low. Sn, however, also a group IVa element, can store up to 2.5 times more Li than graphitic carbon[1]. Several groups have indeed fabricated working electrodes with considerable capacity and cycle life[2–5]. Especially, small Sn particles of the size of several hundreds down to a few nanometers have better cycle life as they are less prone to crack formation and similar structural damages upon volume expansion[6]. Additionally the zoo of possible composite materials such as Sn particles on Carbon nanotubes is a very promising anode material for the future energy storage systems[1,3–5,7–9]. Moreover, Sn is superior to carbon for the sodium battery chemistry[10,11].

Bulk Sn shows a first order phase transition at roughly 13 °C. The so-called tin pest is the result of the transformation of metallic β phase into the non-metallic-zero-gap semiconducting α phase.[15]. This phase transiton not only increases volume by $\sim$30% but also changes the atomic strcuture. Thus, a strong temperature impact on voltage, resistance, and degradation of Sn anodes is expected under operation conditions (typically between –20 and 50°C). In order to understand temperature effects in Sn nanoparticles we have recently studied their stabilities using density functional theory (DFT) by evaluating the impact of surface energies on the total Gibbs free energy. It was found that the metallic β-phase should be increasingly more stable than α-phase of Sn with reducing particle size[16]. Experimental results on pure Sn nanoparticles are however rare and those so far reported are not consistent[17,18].

In this study, we report a theoretical study of structure and stability of nanoparticles of the rarely studied γ polymorph of Sn. This phase is only slightly different than a simple hexagonal structure. We find that this polymorph is structurally very similar and energetically quasi-degenerate to bulk β-Sn for a wide range of exchange-correlation functionals[21], which is also in correspondence to its experimental occurence at temperatures higher than 170 °C[19,20,22]. Here, we show that indeed lower surface energies are obtained for γ-phase compared to β-phase. Therefore, the temperature-size phase diagram shows that γ-Sn is the most stable phase at room temperatures for nanoparticles smaller than 10 nm.. Moreover, our calculations for Sn nanowires with hexagonal cross-section indicates that the surface-induced transition to the γ-phase is not only thermodynamically favorable but also not kinetically limited.

II. METHOD

Total energy calculations are performed within density functional theory (DFT) using the VASP code[23,24]. As the influence of spin-orbit coupling on the energetics is negligible in Sn[25] we only include scalar relativistic effects as by the PAW pseudopotentials[26]. The 4d states are not treated as valence as we expect only influences at higher densities or pressures. Furthermore, we use the PBE[27] exchange correlation functional as it is an appropriate choice for calculating the relative stabilities of Sn polymorphs as well as correct cohesive energies. The bulk structures were modeled by unit cells consisting of eight atoms with a high accuracy of $\sim$0.3 meV/atom obtained by using a plane wave cutoff of 500 eV and k-point density of $> 7 \cdot 10^5 \text{Å}^3$. For the surface energy calculations we

reduced the accuracy to ∼1 meV/atom by using a plane wave cutoff of 220 eV and k-point density of $\sim 1.4 \cdot 10^5 \text{Å}^3$. No significant difference in the results of the present work were observed for the two levels of accuracy.

We evaluate the stability of particles of a given shape by means of their Gibbs free energy per atom[16]

$$g = g_{\text{bulk}}(p,T) + \frac{3\bar{\gamma}}{\rho r} = g_{\text{bulk}}(p,T) + \bar{\gamma} \cdot \sqrt[3]{\left(\frac{6}{\rho}\right)^2 \frac{\pi}{N}}. \quad (1)$$

Here $g_{\text{bulk}}(p,T)$ is the Gibbs free energy per atom in the bulk phase and $\bar{\gamma}$ is the effective, averaged surface energy. The Gibbs free energy per atom in the bulk phase $g_{\text{bulk}}(p,T)$ is obtained within the quasi-harmonic approximation. In a first step, density functional perturbation theory (DFPT) calculations of phonon force-constant matrices were performed using the VASP code for a set of hydrostatically-deformed cells. In a second step, vibrational free energies $F(T,V)$ were extracted from the force-constant matrices using the `phonopy` package[29]. In a third step we obtained the temperature-dependent volume $V_0(T)$ at pressure $p_0 = 1$ bar by solving

$$p_0 = -\partial F(T,V)/\partial V|_{V=V_0(T)} \quad (2)$$

for various temperatures T. Finally, the temperature variation of the Gibbs free energy per cell at fixed pressure p_0 is determined by evaluating

$$G_{\text{cell}}(T,p_0) = F(T,V_0(T)) + pV_0(T), \quad (3)$$

and the Gibbs free energy per atom g_{bulk} is obtained by normalization with the number of atoms in the cell.

The effective, averaged surface energy $\bar{\gamma}$, is defined such that a spherical particle with this surface energy and the nanoparticle of given shape have the same total surface energy for a given volume. r corresponds to the radius of the spherical particle and is related to the total number of atoms N by $N = \frac{4}{3}r^3\pi \cdot \rho$, where ρ is the atomic density of the polymorph (more details in Ref. 16). Specific surface energies γ_i were calculated within the slab approach by

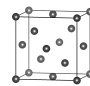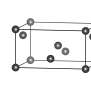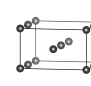$$\gamma \approx \frac{E_{\text{slab}}^{\text{tot}} - N_{\text{Sn}}E_{\text{bulk}}^{\text{tot}}}{2A}, \quad (4)$$

where $E_{\text{slab}}^{\text{tot}}$, A, and N_{Sn} are total energy, the surface area, and the number of Sn atoms in the slab, while $E_{\text{bulk}}^{\text{tot}}$ is the total energy of bulk Sn per atom. Convergence studies for the reported surface energies indicated an accuracy of ∼0.5 meV/Å^2.

III. RESULTS

The calculated bulk properties of α, β, and γ-Sn are tabulated in table I. We find, in agreement with Ref. 19, that the γ-Sn polymorph is expected to have similar stability as β-Sn. When vibrations are included, the bulk

$\alpha \to \beta$ phase transition temperature is reproduced qualitatively correct, however, within PBE, the γ-Sn structure was found even more stable than β-Sn. On the other hand a small correction to the absolute values of PBE bulk energies of -12 meV (-2 meV) for β-Sn (γ-Sn) results in accurate values for the bulk transition temperatures. Such a correction is necessary as DFT can have problems to reproduce the correct relative phase stability[30,31], especially when different bonding types are involved, as is the case here, where covalent (α) and metallic bonding (β, γ) compete. We tested also other functionals and found inferior behavior.

Table I. Structures and properties of different Sn polymorphs. A conventional unit cell was chosen for γ-Sn for a better comparison with the β structure.

	α-Sn	β-Sn	γ-Sn
a (Å)	6.65	5.95	6.16
b (Å)	6.65	5.95	5.64
c (Å)	6.65	3.21	3.27
ρ (atoms/Å^3)	0.0272	0.0352	0.0352
$E_0 - E_0(\alpha\text{-Sn})$ (meV)	0	39.0	38.6

A. Surface properties of γ-Sn

The rhombic γ-Sn lattice parameters are very close to those of β-Sn. The unit cell is depicted in table I. It is obviously also closely related to a conventional hexagonal cell where the hexagonal plane lies in the **bc** plane and the hexagonal **z** direction along the **a** direction of γ-Sn. The nearest neighbors of each Sn atom in γ-Sn are the two along the **a** direction (d ≈ 3.08Å) and the 6 in the **bc** plane (d ≈ 3.26Å).

The calculated surface energies for several possible low-index terminations of γ-Sn are tabulated in table II and the most important surface terminations are depicted in Fig. 1. The lowest energy terminations of γ-Sn have surface energies of only ≈ 22 meV/Å^2 and they correspond to the possible bisections of the hexagonal structure without breaking the bonds to the two closest nearest neighbors along the **a** axis. The surface energies increase in the order $\{010\} \to \{012\} \to \{021\} \to \{001\}$ which is in line with the fact that these surfaces correspond to perfect and increasingly stepped "hexagonal" surfaces (see Fig. 1 a–c). The cost of step formation seems to be remarkably low in $\{012\}, \{021\}, \{001\}$. The γ-Sn surfaces that cut through the bonds perpendicular to the hexagonal plane, e.g. $\{122\}$, $\{102\}$ and $\{100\}$, have higher surface energies between 23.7 and 24.6 meV/Å^2, which are in the same range as the most stable surface of β-Sn, namely

Table II. Surface energies of γ-Sn and relative contributions of surfaces to the Wulff shape.

{hkl}	{010}	{012}	{021}	{001}	{122}	{102}	{100}	{111}	{120}	{212}	{101}	{210}	{221}	{110}	{201}
							γ-Sn surfaces								
γ_s (meV/Å^2)	21.7	21.7	22.2	22.5	23.7	24.5	24.6	25.4	26.0	27.3	27.5	27.6	27.8	28.0	28.7
% of Wulff shape	8.4	31.9	-	1.5	7.2	8.8	13.3	12.3	-	-	-	12.9	2.7	-	1.1

(100) with a surface emergy of 23.6 meV/Å^2[16]. In general, surface relaxations on γ-Sn surfaces are smaller than those on β-Sn counterparts.

B. Wulff shape and nanoparticle stability at 0 K.

In order to determine the lowest energy structure of Sn nanoparticles we constructed the Wulff shapes as drawn in Fig. 2 in which high-surface-area faces are colored in blue and green.

The Wulff shape of α-Sn is rather simple, dominated by the reconstructed {100} (blue) and {111} (green) surfaces, which together comprise 73% of the total surface. The Wulff shape of β-Sn is dominated by the {100} (blue), {101} (green) and {201} terminations (see Fig. 2 b), constituting of 70% of the total surface area. It resembles a pyramidally capped cube. For γ-Sn we again adopted our approach to interpret surface energies as if they were obtained from calculations of a conventional hexagonal cell.

This allows us to apply hexagonal symmetry operations and evaluate surface energies of many more than just the calculated ones. As a result the constructed Wulff-shape has a perfect hexagonal symmetry (see Fig. 2 c). This is not only conventient but also necessary to understand e.g. the relative importance of several γ-Sn high-index surfaces, as these correspond often to very simple hexagonal surfaces. We provide a mapping of the

(hkl) notation of γ-Sn to a hexagonal primitive unit cell notation $\{hkl\}^\gamma \rightarrow \{hkl\}^{hex}$ in the supporting information (SI). The γ-Sn Wulff shape is slightly elongated in the **a** direction due to the comparably large {100} (blue) surface energy. The shape resembles a cylinder which is a result of step formation energies on {100} and vicinal surfaces (green).

C. Nanoparticle stability at T > 0 K.

The phase diagram for Sn nanoparticles can be obtained from equation 1 as a function of temperature and number of atoms. The averaged surface energies $\bar{\gamma}$ of equation 1 were determined by averaging the surface energies appropriately across these Wulff-shapes. The values are tabulated in table III.

The temperature-size phase diagram of Sn nanoparitlces are illustrated in Fig. 3. The range of typical battery operation temperatures (-20°C – +50°C) is shaded in green. The graphs were obtained by mapping the number of Sn atoms N_{Sn} in the range $[2000, \infty[$ onto $[0, 1[$ via: $N_{Sn} \rightarrow \left(1 - \left[\frac{\log(2000)}{\log(N_{Sn})}\right]^5\right)^3$ and the effective diameter corresponds to spherical β-phase particles with equivalent atom number.

As stated before we had to shift the absolute values of the free energies of β and γ-Sn by -12 meV and -2 meV respectively to obtain the correct bulk phase transition temperatures. For small particle sizes the large surface energy contributions stabilizes the β and γ phases. The bulk behavior is basically observed for particles larger than 100 nm.

For nanoparticle sizes below 50 nm, the α-β phase transition temperature drops significantly so that the tin pest
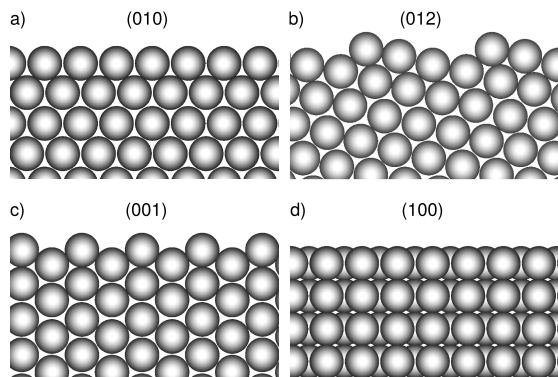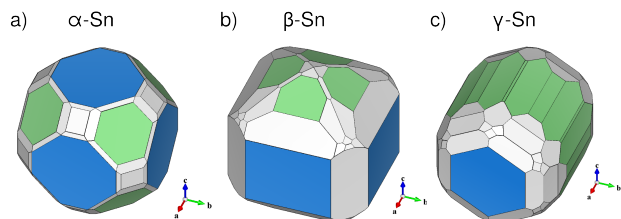

Figure 1. Side views of structures of the most important surface terminations of γ-Sn (relaxed structures). a) (010), b) (012) and c) (001) belong to the very stable surface family which involves no bond breaking along the a axis (along the c axis for the coresponding quasi-hexagonal structure). d) (100) is perpendicular to the surfaces a–c. The calculated surface freenergies are listed in table II.

Figure 2. Wulff shapes of α, β, and γ-Sn nanoparticles. The most important (lowest energy) surfaces are depicted in blue and green. {100} surfaces (blue) are important for all polymorphs. They are the lowest energy terminations for α and β-Sn. For γ-Sn {010} and its vicinal surfaces (green) are more favorable.

Table III. Effective surface energies $\bar{\gamma}$ of Wulff shaped nanoparticles of different possible Sn phases (see Fig. 2).

	α-Sn	β-Sn	γ-Sn
$\bar{\gamma}$(meV/Å^2)	34.1	27.0	24.8

is inhibited within the operating temperature range. Furthermore, nanoparticles of sizes below ≈ 11 nm should only be stable as γ-Sn or β-Sn at any temperature. We find that the β-γ transition temperature, which is $\approx 170°$C in the bulk form, drops to room temperatures for Sn nanoparticles of smaller 10 nm. Therefore, small Sn nanoparticles are

which are in fact less important for the electrode performance since the change in electronic and atomic structure is much less dramatic as in the case of α-β.

D. Sn nanowires

In order to confirm the extrapolations from the Wulff shaped nanoparticles we also performed computations for real nanostructures. We focus on a nanowire geometry since it is more suited to model using periodic DFT codes. By construction the simulated nanowires are infinitely extended along the a-direction. A topologically equivalent hexagonal cross section was assumed for the β and γ-Sn nanowires with (101) and β-Sn(010) surfaces and γ-Sn(010) surfaces exposed, respectively (see Fig. 4). The hexagon was chosen such that the β-Sn nanowire cross section is minimizing the total surface energy of the enclosing (101) and (010) surfaces. The nanowire consisits
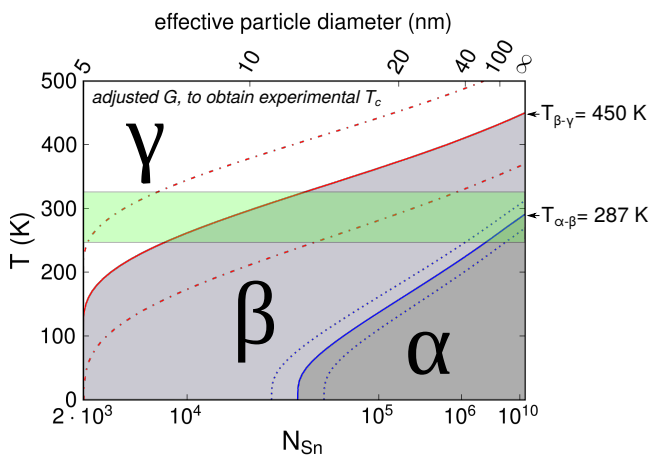

Figure 3. Temperature-size phase diagram of Sn nanoparticles. The effective particle diameters correspond to equivalent spherical β-Sn particles with the same number of Sn atoms. The stability lines are obtained from DFT-derived free energies empirically shifted to reproduce the experimental bulk transition temperatures with the dashed lines indicating the effect of a 2 meV error. Typical battery operation temperatures are shaded with a green area.

of 226 atoms and its diameter is approximately 3.5 nm. The equilibrium bulk lattice parameters are indicated in Fig. 4 as dotted vertical lines.

We find that the β-Sn nanowire with β bulk lattice parameter is clearly higher in energy than the equivalent γ-Sn one, as expected from the lower surface energy of γ-Sn(010). On the other hand, if we extend the a lattice parameter of the β-Sn nanowire (red squares) towards the γ-Sn equilibrium value the total energies dramatically decrease and a minimum energy close to the γ-Sn lattice parameter is obtained. With this lattice parameter, the atomic structures of β-Sn and γ-Sn nanowires are found to be practically equivalent. However there is a slight energy discrepancy of $\approx$120 meV between the β and γ nanopaticles truncated from the bulk (red and blue curve).

In principle, there should be no energy difference between these structures since we allowed all lateral degrees of freedom to relax. This indicates a high degree of frustration. To overcome this effect we applied an $ab-initio$ molecular dynamics annealing procedure as explained in the supporting information. The calculated energies for different lattice parameters (green curve) as well as the minimum-energy relaxed structures are illustrated in 4. It can be seen that it is not possible to assign a clear phase β or γ to those structures due to the large variations of structural configurations near surfaces. Nevertheless, the
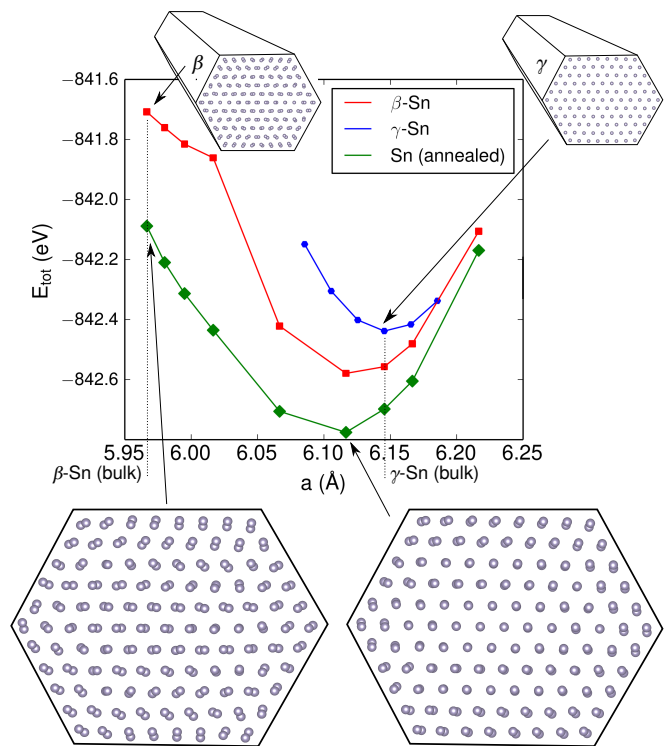

Figure 4. Total energy of DFT-relaxed ($T = 0, p = 0$) β-Sn (red curve with squares) and γ-Sn as well as annealed ($T = x, p = 0$) nanowires with hexagonal cross-sections as function of lattice parameter a.

minimum energy structure is obviously closely related to γ-Sn, looking at the center of the nanaowire cross section. This is in line with the observed low surface energies of γ-Sn(010) that drives the β-Sn nanowire into a γ-Sn-like nanowire. Furthermore, we do not find a kinetic barrier for this transition (see Fig. 4). The results are in agreement with the reported elongation of β-Sn nanowires[32]. we however show that the effect goes beyond a pure relaxation of surface stress and is rather induced by the more stabilty of the γ-phase with respect to the β phase in Sn nanostructures.

IV. CONCLUSION

In this work, we studied structure, stability, and phase transition in Sn nanoparticles and nanowires. According to the calculated temperature-size phase diagram, the phase stability of Sn changes dramatically by nanoscaling. It is found that the $\alpha - \beta$ phase transition temperature changes from 13°C to below -20°C in nanoparticles of sizes smaller than 50 nm. The β-Sn nanoparticles are metallic and exhibit a higher density which is favorable in terms of conductivity and potential volumetric energy density. On the other hand α-Sn exhibits the more open diamond lattice structure which might be favorable in terms of kinetic diffusion barriers. Which property is more relevant for anode performance is still an open question. Surface stabilization by adatoms or molecules might as well be used e.g. to stabilize the α phase. We also found that that surfaces should increase the stability of γ-Sn such that its stability range is shifted from high temperatures (close to the melting point) to room temperatures for nanoparticles smaller than 10 nm. The stabilization can be understood from the increased coordination number of Sn atoms in the γ polymorph (2+6 coordination), which makes bond cutting at surfaces easier than in β-Sn (4+2 coordination), as even surface atoms in γ-Sn can still retain e.g. the same coordination as in bulk β-Sn. We hope that this work motivates new research efforts to study phase-sensitivity in the performance of nanostructured anode materials.

V. ACKNOWLEDGEMENTS

* payam.kaghazchi@fu-berlin.de

[1] J. W. Wang, X. H. Liu, S. X. Mao, J. Y. Huang, *Nano Lett.* **12**(11), 5897 (2012).

[2] D. Larcher, et al., *J. Mater. Chem.* **17**, 3759 (2007).

[3] Y. Yu, L. Gu, C. Zhu, P. A. van Aken, J. Maier, *JACS* **131**(44), 15984 (2009), PMID: 19886691.

[4] H. Zhu, et al., *Nano Lett.* **13**(7), 3093 (2013).

[5] J. Qin, et al., *ACS Nano* **8**(2), 1728 (2014).

[6] N.-S. Choi, Y. Yao, Y. Cui, J. Cho, *J. Mater. Chem.* **21**, 9825 (2011).

[7] Y. Zou, Y. Wang, *ACS Nano* **5**(10), 8108 (2011).

[8] X. Zhou, J. Bao, Z. Dai, Y.-G. Guo, *J. Phys. Chem. C* **117**(48), 25367 (2013).

[9] Y. Xu, et al., *Phys. Rev. Lett.* **111**, 136804 (2013).

[10] M. D. Slater, D. Kim, E. Lee, C. S. Johnson, *Adv. Funct. Mater.* **23**(8), 947 (2013).

[11] B. Wang, B. Luo, X. Li, L. Zhi, *Materials Today* **15**(12), 544 (2012).

[12] M.-F. Ng, T. L. Tan, *Nano Lett.* **13**(10), 4951 (2013).

[13] S. Küfner, J. Furthmüller, L. Matthes, M. Fitzner, F. Bechstedt, *Phys. Rev. B* **87**, 235307 (2013).

[14] S. Küfner, J. Furthmüller, L. Matthes, F. Bechstedt, *Nanotechnology* **24**(40), 405702 (2013).

[15] G. Busch, R. Kebn, vol. 11 of *Solid State Physics*, pp. 1 – 40. Academic Press (1960).

[16] N. G. Hörmann, A. Gross, P. Kaghazchi, *Phys. Chem. Chem. Phys.*, (2015) *accepted*.

[17] Y. Xu, et al., *Nano Lett.* **13**(2), 470 (2013).

[18] H. S. Im, et al., *ACS Nano* **7**(12), 11103 (2013).

[19] B. Wehinger, et al., *Journal of Physics: Condensed Matter* **26**(11), 115401 (2014).

[20] C. L. Mantell, *Tin*. New York: Reinhold Publishing Corp. (1949).

[21] J. Rohrer, N. G. Hörmann, A. Gross, P. Kaghazchi, *in preparation*.

[22] N. Burns, *Journal of Failure Analysis and Prevention* **9**(5), 461 (2009).

[23] G. Kresse, J. Furthmüller, *Phys. Rev. B* **54**, 11169 (1996).

[24] G. Kresse, J. Furthmüller, *Comput. Mater. Sci.* **6**(1), 15 (1996).

[25] N. E. Christensen, M. Methfessel, *Phys. Rev. B* **48**, 5797 (1993).

[26] J. Hafner, *J. Comput. Chem.* **29**, 20442078 (2008).

[27] J. P. Perdew, K. Burke, M. Ernzerhof, *Phys. Rev. Lett.* **77**, 3865 (1996).

[28] P. Pavone, S. Baroni, S. de Gironcoli, *Phys. Rev. B* **57**, 10421 (1998).

[29] A. Togo, F. Oba, I. Tanaka, *Phys. Rev. B* **78**, 134106 (2008).

[30] C. Fang, M. van Huis, H. Zandbergen, *Phys. Rev. B* **80**, 224108 (2009).

[31] M. E. Arroyo-de Dompablo, A. Morales-Garca, M. Taravillo, *The Journal of Chemical Physics* **135**(5), (2011).

[32] Y.-S. Kim, S. M. Lee, J. Y. Song, *Appl. Surf. Sci.* **256**(11), 3603 (2010).